Sustainable S cathodes with synergic electrocatalysis for room-temperature Na-S batteries

Hanwen Liu,[a] Wei-Hong Lai,[a] Yaru Liang,[b] Xin Liang,[c] Zi-Chao Yan,[a] Hui-Ling Yang,[a] Yao-Jie Lei,[a] Pei Wei,[d] Si Zhou,[a,d] Qin-Fen Gu,[e] Shu-Lei Chou,[a] Hua Kun Liu,[a] Shi Xue Dou,[a] Yun-Xiao Wang*[a]

[a] Institute for Superconducting and Electronic Materials, Australian Institute of Innovative Materials, University of Wollongong, Innovation Campus, Squires Way, North Wollongong, NSW 2500, Australia
[b] Powder Metallurgy Research Institute, State Key Laboratory of Powder Metallurgy, Central South University, Lushan South Road, Changsha, 410083, China
[c] School of Materials Science and Engineering; Engineering Research Center of High Performance Copper Alloy Materials and Processing, Ministry of Education, Hefei University of Technology, Hefei 230009, Anhui, P. R. China
[d] Key Laboratory of Materials Modification by Laser, Ion and Electron Beams, Dalian University of Technology, Ministry of Education, Dalian 116024, China
[e] Australian Synchrotron 800 Blackburn Road, Clayton, VIC 3168, Australia

Table of Contents

1. Supplementary Figures

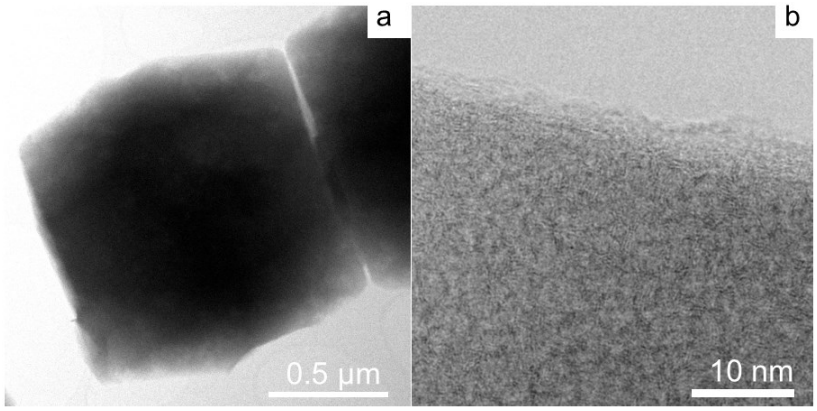

Figure S1: STEM images of C@S.

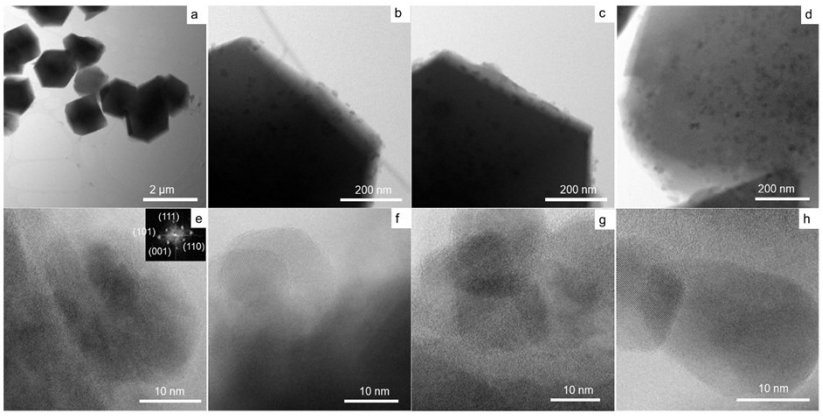

Figure S2: STEM images of ZnS/C@S.

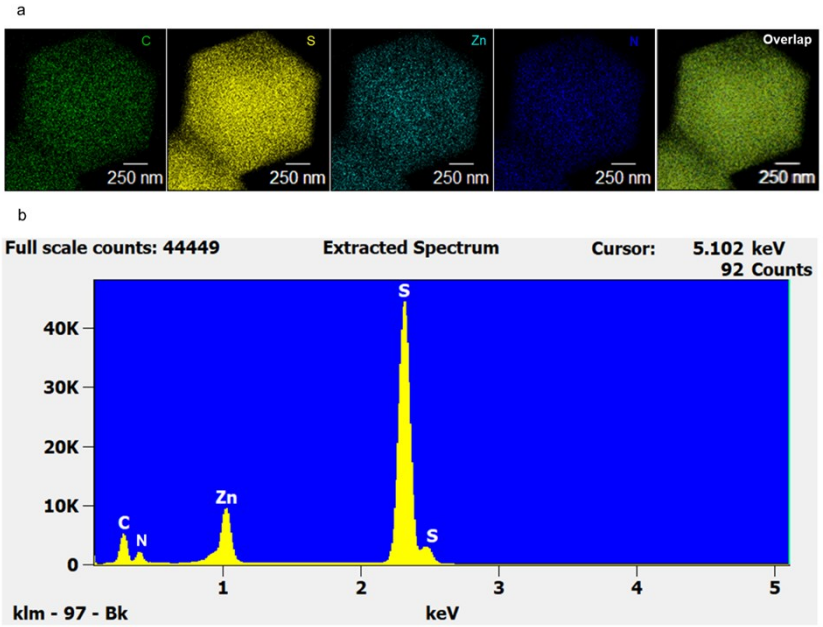

Figure S3: (a) EDS mapping of ZnS/C@S. (b) Elemental calculations of ZnS/C@S that C: 9 % N: 4.3 % Zn: 12.7 % S: 74 %.

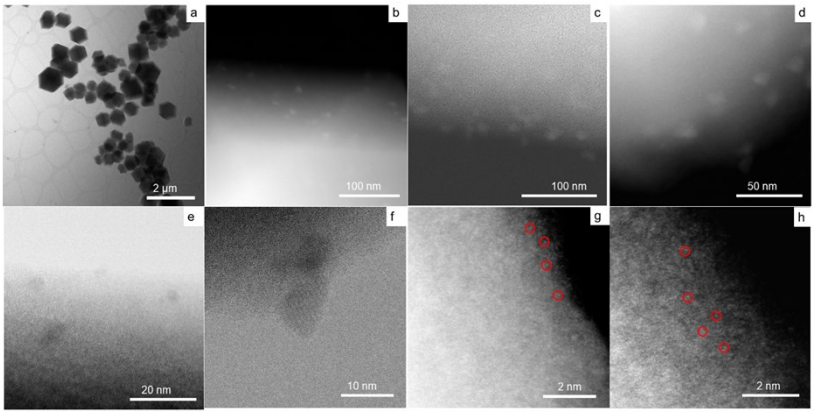

Figure S4: STEM images of Co_1-ZnS/C@S.

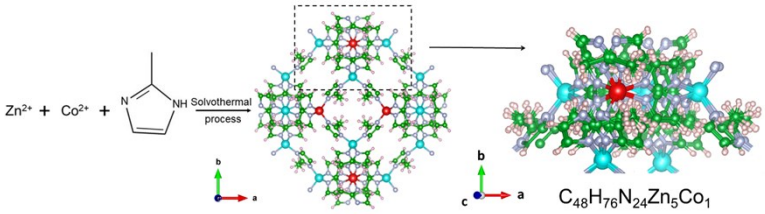

Figure S5: The doping of Co^{2+} which replaces part of Zn^{2+} and coordinates with 2-methylimidazole.

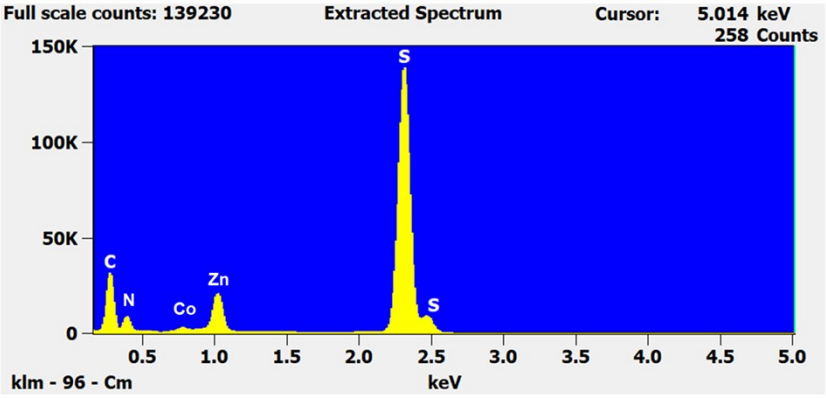

Figure S6: the elemental calculations of Co_1-ZnS/C@S that C: 12.1 % N: 3.9% Co: 1.8 % Zn: 8.3 % S: 73.9 %.

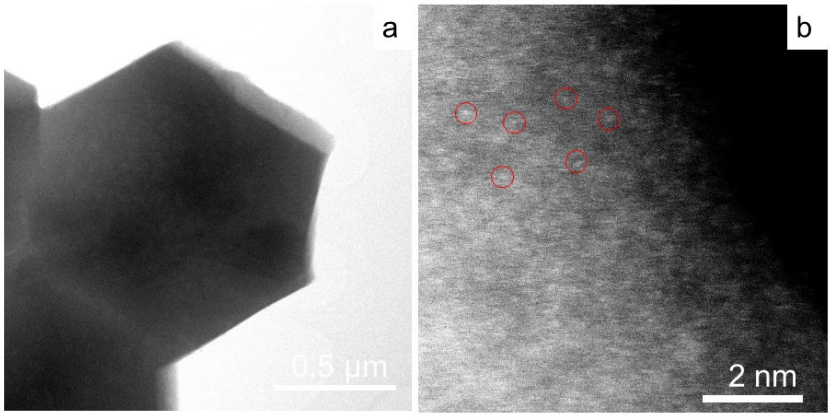

Figure S7: STEM images of Co_1/C@S.

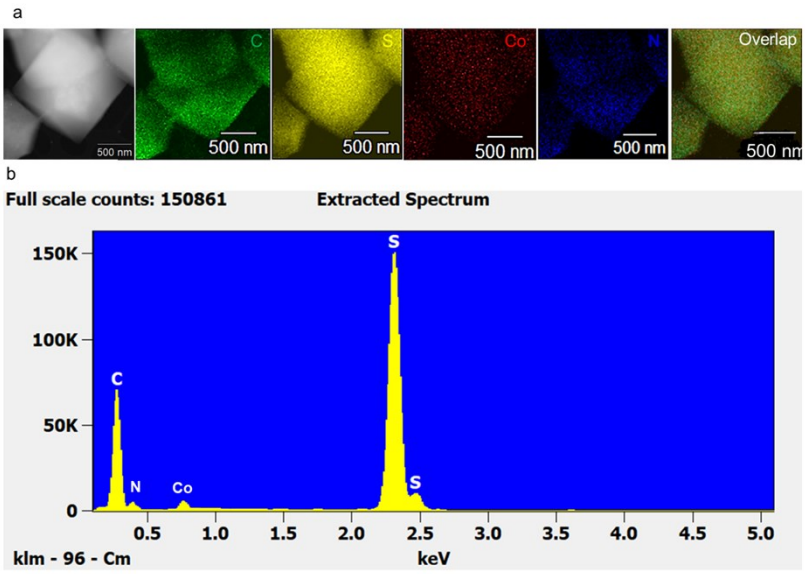

Figure S8: (a) EDS mapping of Co_1/C@S. (b) Elemental calculations of ZnS/C@S that C: 19 % N: 2.3 % Co: 2.1 % S: 76.6 %.

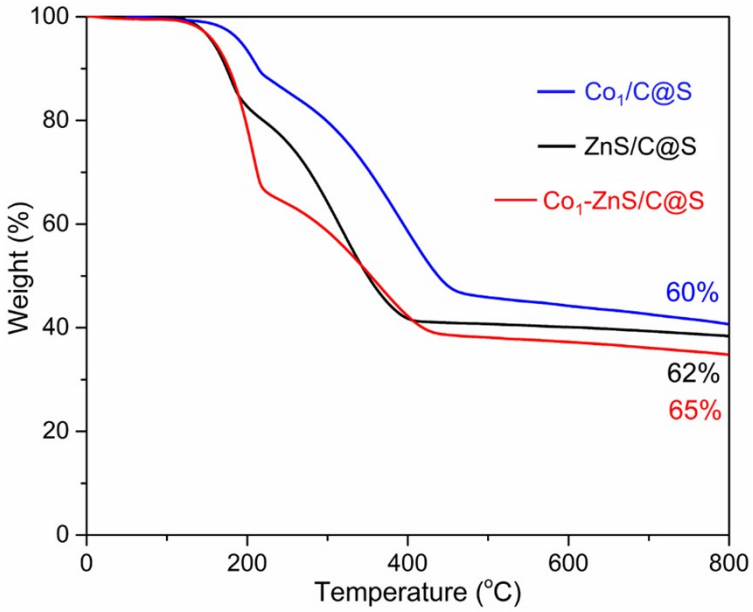

Figure S9: TGA test for Co_1/C@S, Co_1-ZnS/C@S and ZnS/C@S indicates sulfur account for 60 %, 65 % and 62 % in corresponding samples.

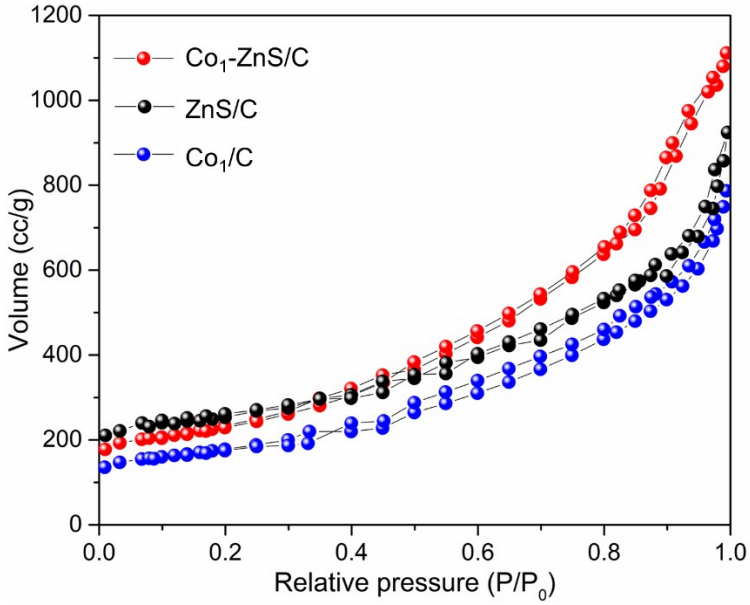

Figure S10: BET analysis confirms the specific area of Co_1/C, Co_1-ZnS/C and ZnS/C with 756, 1012 and 928 $m^2\ g^{-1}$ respectively.

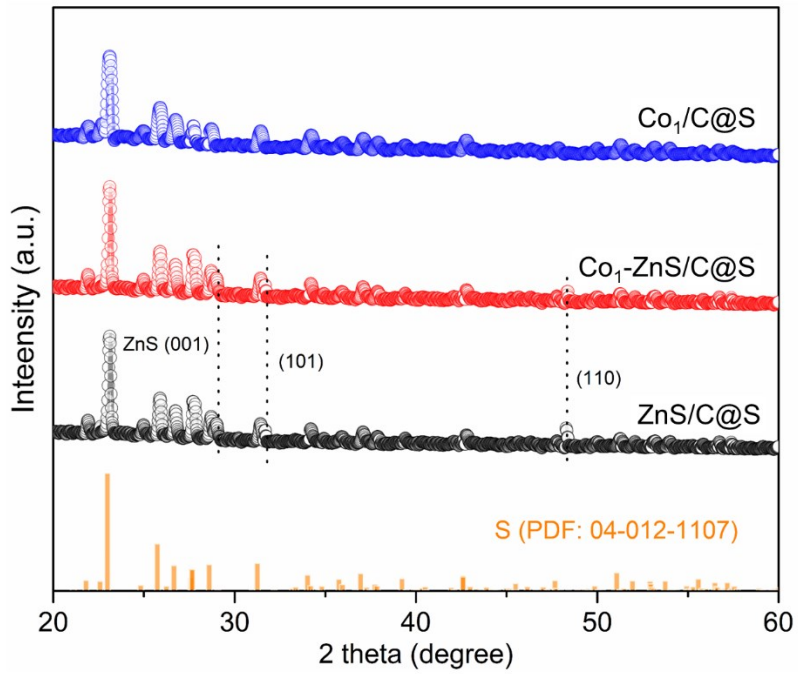

Figure S11: XRD confirms crystalline S (JCPDF: 04-012-1107) and planes of crystalline ZnS (001), (101) and (110)

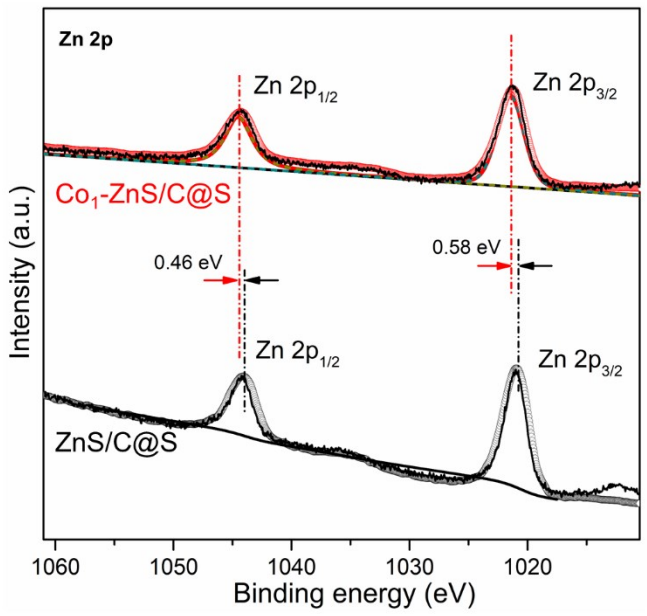

Figure S12: XPS of Co_1-ZnS/C@S and ZnS/C@S in Zn 2p region.

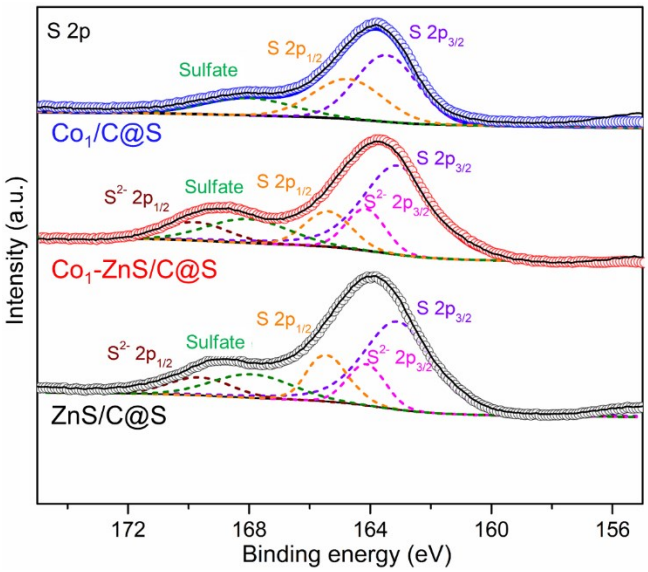

Figure S13: XPS of Co_1/C@S, Co_1-ZnS/C@S and ZnS/C@S in S 2p region.

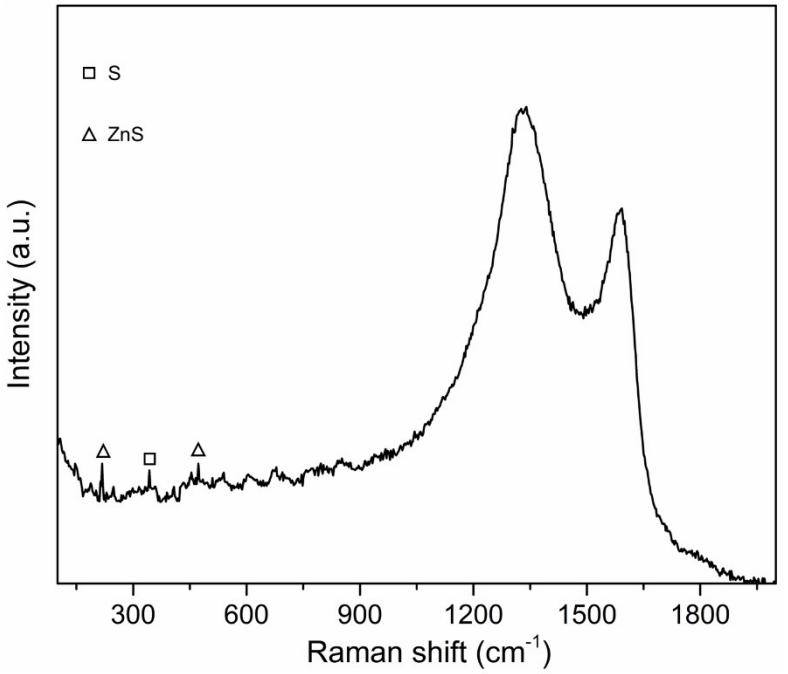

Figure S14: Raman spectra of Co_1-ZnS/C@S.

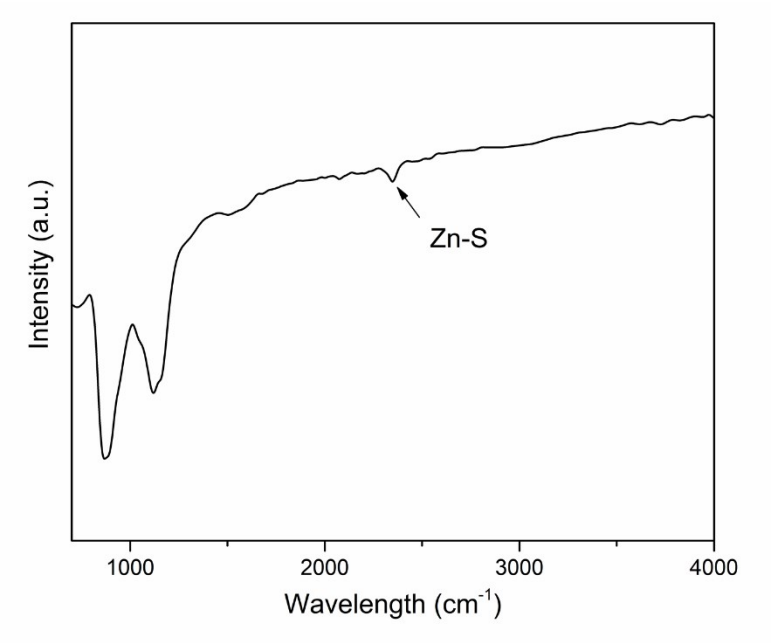

Figure S15: FT-IR spectra of Co_1-ZnS/C@S.

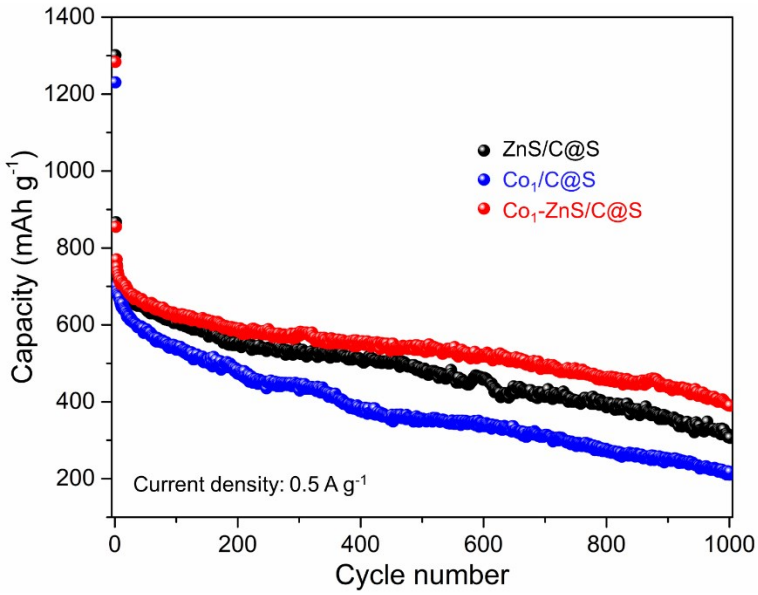

Figure S16: Cycle performance of Co_1/C@S, Co_1-ZnS/C@S and ZnS/C@S at 0.5 A g^{-1}.

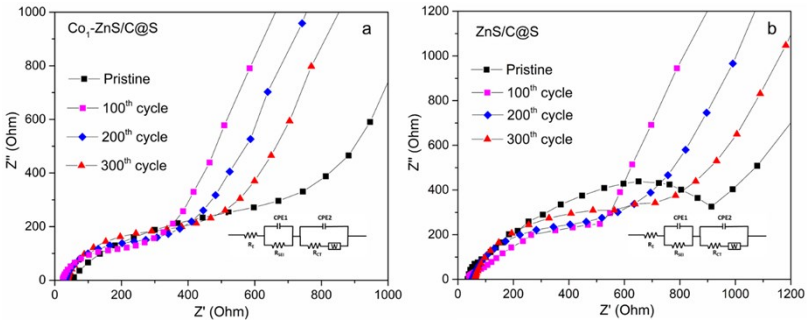

Figure S17: EIS and randles equivalent circuit of (a) Co_1-ZnS/C@S and (b) ZnS/C@S.

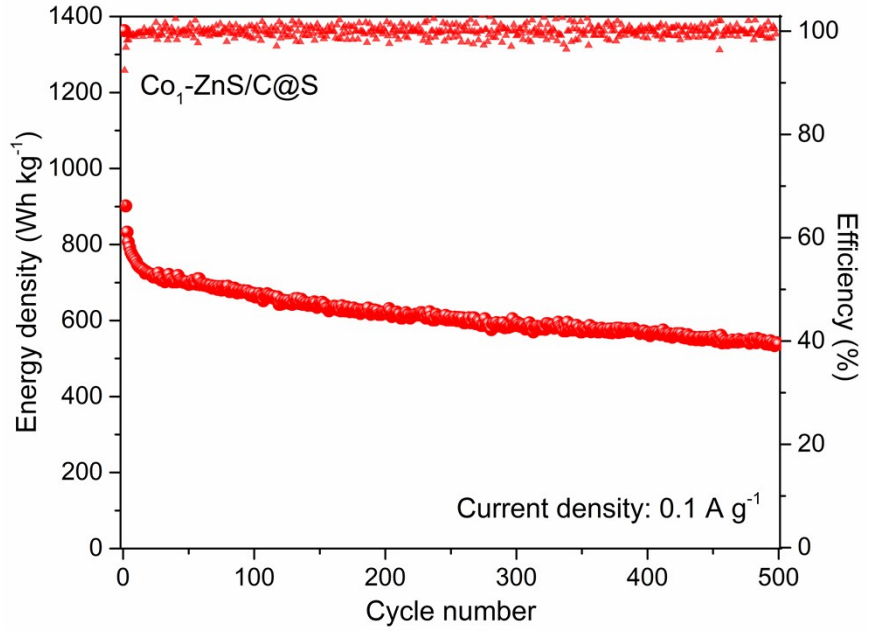

Figure S18: Energy density of Co_1-ZnS/C@S in the voltage range of 0.8-2.8 V materials at current density of 0.1 A g^{-1}. After 500 cycles, there is still 541 Wh kg^{-1} of energy density and its retention reaches to 60.1 % after activation.

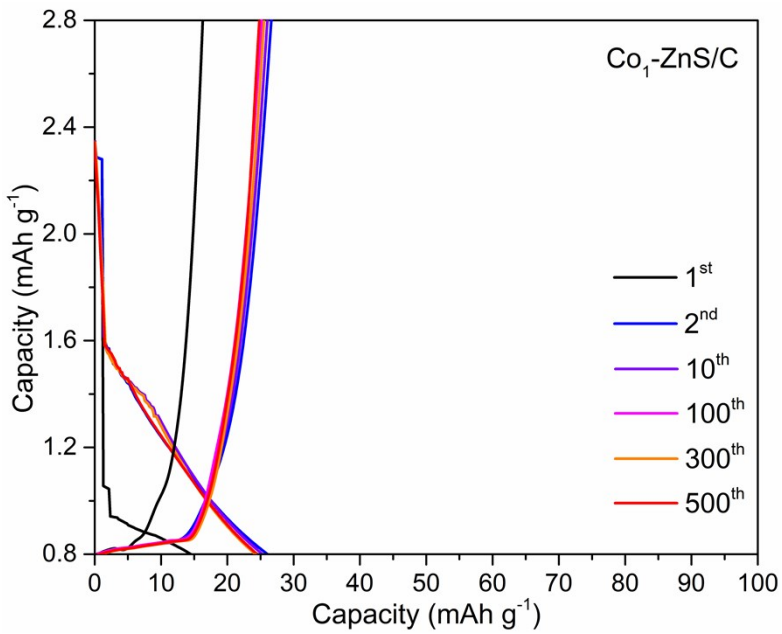

Figure S19: Discharge/charge curves of (a) Co_1-ZnS/C at 0.1 A g^{-1} within voltage range from 0.8 to 2.8 V.

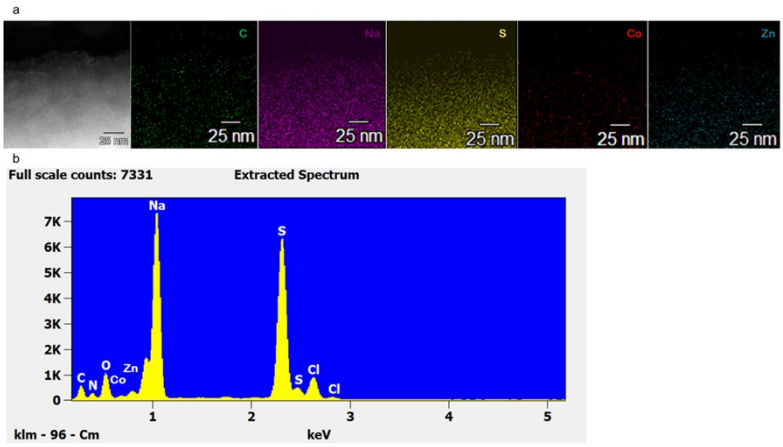

Figure S20: (a) EDS mapping and (b) element distribution of Co_1-ZnS/C@S after 500 cycles.

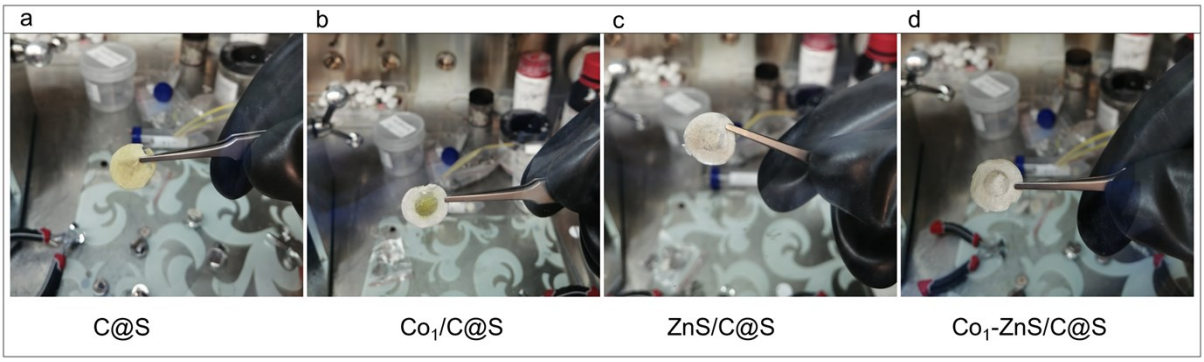

Figure S21: (a)-(d) images of separator in C@S, Co_1/C@S, ZnS/C@S and Co_1-ZnS/C@S electrodes after 500 cycle.

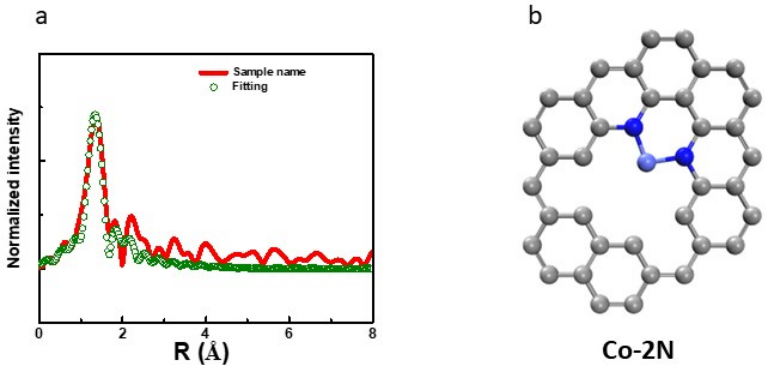

Figure S22: (a) EXAFS data of Co_1-ZnS/C@S and its fitting result. (b) The coordination model between Co atom and N on carbon layer based on the fitting result.

Table S1. EXAFS fitting parameters at the Co K-edge for various samples

Shell	N [a]	R (Å) [b]	σ^2 (Å$^2 \cdot 10^{-3}$) [c]	*R* factor (%)
Co-N	1.5	1.66	2.9	0.2

[a] *N*: coordination numbers; [b] *R*: bond distance; [c] σ^2: Debye-Waller factors; *R* factor: goodness of fit.

*S*02 were set as 0.9 for Co-N, which were obtained from the experimental EXAFS fit of reference CoPc by fixing CN as the known crystallographic value and was fixed to all the samples.

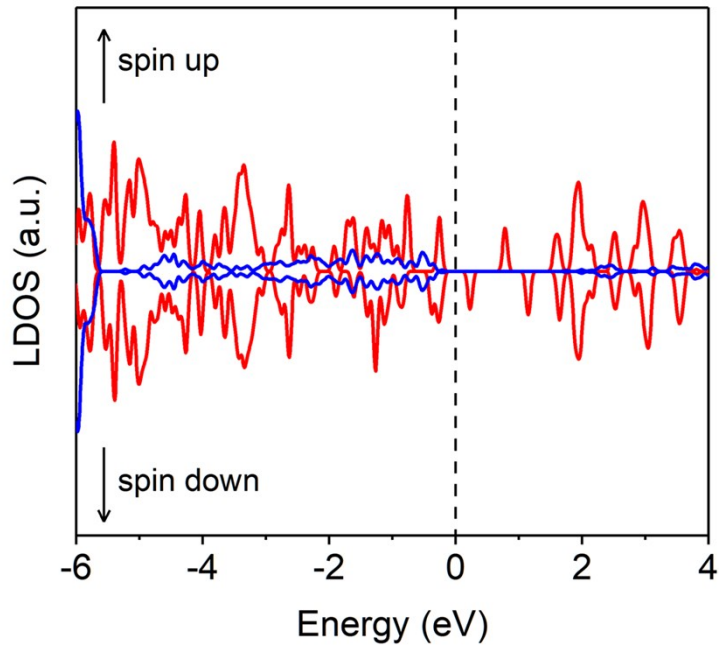

Figure S23: Local density of states (LDOS) for ZnS(110) (red) and Co_1@NG (blue). The black dashed line indicates the Fermi level. Co_1@NG was modelled by a single Co atom bonding with two N atoms embedded in the divacancy of graphene monolayer, which is based on our experimental XAS fitting that Co−N coordination number is about 2.

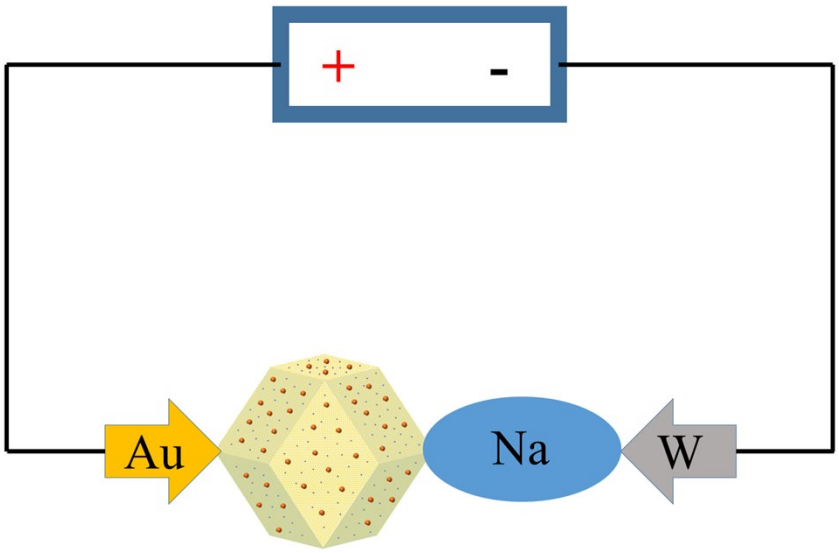

Figure S24: Schematic representation for the in-situ TEM configuration.

2. EXAFS fitting and DFT calculations

XAFS Analysis and Results.

The XAS spectra were collected by use of the APS, an Office of Science User Facility operated for the DOE Office of Science by Argonne National Laboratory. The acquired EXAFS data were processed according to the standard procedures using the ATHENA module implemented in the IFEFFIT software packages. The k3-weighted EXAFS spectra were obtained by subtracting the post-edge background from the overall absorption and then normalizing with respect to the edge-jump step. Subsequently, k3-weighted $\chi(k)$ data of Fe *K*-edge were Fourier transformed to real (R) space using a hanning windows (dk=1.0 $Å^{-1}$) to separate the EXAFS contributions from different coordination shells. To obtain the quantitative structural parameters around central atoms, least-squares curve parameter fitting was performed using the ARTEMIS module of IFEFFIT software packages.[1-3]

DFT calculations

DFT calculations were performed by the Vienna ab initio simulation package (VASP), using the planewave basis set with energy cutoff of 550 eV, the projector augmented wave (PAW) potentials, and the generalized gradient approximation proposed by Perdew, Burke and Ernzerhof (GGA-PBE) for the exchange-correlation functional. Slab models were used for the ZnS (110) surfaces with 4, 4 and 6 Zn–S layers, and the supercells consist of 3 × 3, 4 × 4 and 3 × 4 unit cells, respectively. The ZnS (110) surface was modelled by a slab of 4 S–Zn–S layers and 3 × 3 unit cells. A vacuum region of 16 Å was applied for the vertical direction. For all these supercells structures, the lateral dimension ranges from 15.25 to 16.33 Å. The Brillouin zone was sampled by a 2 × 2 × 1 uniform k point mesh. With constrained lattice, the model structures were optimized for the ionic and electronic degrees of freedom, using thresholds for the total energy of 10–4 eV and force of 0.02 eV/Å. During the structural relaxation, the bottom two layers of metal and S atoms were fixed to mimic a semi-infinite solid. Grimme's semiempirical DFT-D3 scheme of dispersion correction was adopted for better description of the interaction between polysulfides and catalysts. To characterize the catalytic activity of ZnS(110) towards Na-S reactions, the energy diagram for charging (discharging) process in the sodium sulfur battery was calculated by considering the elemental steps below:

$$Na_2S_8 \leftrightarrow 2Na^+ + 2e^- + S_8 \quad (1)$$

$$4/3Na_2S_6 \leftrightarrow 2/3Na^+ + 2/3e^- + Na_2S_8 \quad (2)$$

$$3Na_2S_2 \leftrightarrow 4Na^+ + 4e^- + Na_2S_6 \quad (3)$$

$$8Na_2S \leftrightarrow 8Na^+ + 8e^- + 4Na_2S_2 \quad (4)$$

The overall reaction is

$$8Na_2S \leftrightarrow 16Na^+ + 16e^- + S_8 \quad (5)$$

Following the hydrogen electrode model proposed by J. K. Nørskov,[4] here in sodium sulfur battery, we assume that $Na^+ + e^-$ are in the electrochemical equilibrium with the bulk Na metal. The reaction energy of each elemental step can be obtained by calculating the binding energies of polysulfide species (Na_2S, Na_2S_2, Na_2S_6, Na_2S_8, S_8) on the catalyst.

Based on the above method, the absolute value of energy level of Na_2S_8 during charge in Fig. 3g is the total heat of reaction from step (4) to step (2), that is $8Na_2S \rightarrow 14Na^+ + 14e^- + Na_2S_8$. The heat of reaction is $\Delta H = E(Na_2S_8) + 14E(Na) - 8E(Na_2S) = -14.72$ eV, where $E(Na_2S_8)$ and $E(Na_2S)$ are the energies of Na_2S_8 and Na_2S species adsorbed on the catalyst, respectively; $E(Na)$ is the energy of a Na atom in the form of Na solid.

References:

1. B. Ravel and M. Newville, *J. Synchrotron Radiat.*, 2005, **12**, 537-541.
2. D. Koningsberger and R. Prins, 1988.
3. J. J. Rehr and R. C. Albers, *Rev. Mod. Phys.*, 2000, **72**, 621.
4. J. K. Nørskov, T. Bligaard, A. Logadottir, J. Kitchin, J. G. Chen, S. Pandelov and U. Stimming, *J. The Electrochem. Soc.*, 2005, **152**, J23.